Journal of Molecular Spectroscopy **201,** 83–94 (2000)
doi:10.1006/jmsp.2000.8065, available online at http://www.idealibrary.com on IDEAL®

The Intensities of Methane in the 3–5 μm Region Revisited

L. Féjard,* J. P. Champion,* J. M. Jouvard,† L. R. Brown,‡ and A. S. Pine§

**Laboratoire de Physique (Unité associée au C.N.R.S.), Université de Bourgogne, 9 Avenue A. Savary, B.P. 47870, 21078 Dijon, France; †Laboratoire de Thermomécanique, I.U.T., 12 Rue de la Fonderie, 71200 Le Creusot, France; ‡Jet Propulsion Laboratory, California Institute of Technology, Pasadena, California 91109; and §Alpine Technologies, 14401 Poplar Hill Road, Germantown, Maryland 20874*

E-mail: Jean-Paul.Champion@u-bourgogne.fr

Received December 9, 1999

The analysis of the linestrengths of the infrared spectrum of methane (12 and 13) in the 3–5 μm region has been revisited on the basis of new measurements from Fourier transform spectra recorded at Kitt Peak under various optical densities. A simultaneous fit of these new data with previously reported tunable difference-frequency laser data has been done. An effective transition moment model in tensorial form up to the third order of approximation within the Pentad scheme has been used. The standard deviations achieved are very close to the experimental precision: 3 and 1.5%, respectively, for the two sets of data for the $^{12}CH_4$ molecule, representing a substantial improvement with respect to earlier studies. The integrated bandstrengths obtained in the present work differ from previously reported values by factors ranging from -5 to $+6$%. The correction for the ν_3 band, the strongest band of the Pentad system, is $+2$% with respect to the study of Hilico *et al.* [J. C. Hilico, J. P. Champion, S. Toumi, V. G. Tyuterev, and S. A. Tashkun, *J. Mol. Spectrosc.* **168,** 455–476 (1994)].

Key Words: methane; high resolution; infrared; absolute intensities.

1. INTRODUCTION

Precise spectroscopic parameters of methane are required for monitoring purposes in atmospheric physics. Several works have been devoted to the study of the intensities of methane in the 3–5 μm region (*1, 2, 3*). In their theoretical analysis of the ν_3 band intensities, Dang-Nhu *et al.* (*4*) included the interactions with other bands indirectly. However, the first global analysis of the intensities of the Pentad band system of methane (ν_1, ν_3, $2\nu_2$, $\nu_2 + \nu_4$ and $2\nu_4$) in the 3–5 μm region was published in 1983 (*5*). This study used line positions recorded with the FTS at Orsay (*6*) and intensity data taken from the AFGL compilation (*7*). The experimental intensities were laser measurements of Dang-Nhu *et al.* (*4*) for the strongest allowed lines of ν_3 combined with mainly grating data from Toth *et al.* (*8*) for the weaker transitions. The reported rms was 12%. The same data were exploited again in a new analysis of the Pentad of methane published in 1994 (*9*). The use of an improved theoretical model yielded an rms of 8% and confirmed the need for more precise intensity measurements.

The present work was undertaken to provide a better intensity analysis. Series of Fourier transform spectra were recorded at Kitt Peak National Observatory under various optical densities. These new data were combined in a simultaneous fit with measurements from laser spectrometry already reported in the literature (*10, 4, 11, 12*). To complement the analyses of the line positions of the isotopic species $^{12}CH_4$ (*9*), $^{13}CH_4$ (*13*), and the recent global study of $^{12}CH_3D$ (*14*), this work achieves a significant improvement of the modeling of the infrared spectrum of methane in the 3–5 μm region.

2. THEORY

The theoretical model used in the present work is based on the general tensor approach of the energies and intensities of spherical-top molecules. It is already described in the literature (*15*). Some details on the application to the pentad of methane were given in (*9*) and will not be repeated here. The modeling of linestrengths require the eigenvectors of the lower and upper states of the transitions under consideration. We essentially used the eigenvectors from the work of Hilico *et al.* (*9*) except that in order to produce reliable absolute spectroscopic parameters we have reconsidered the consistency of the measured line positions presently available.

In our model, all possible vibration–rotation operators (Hamiltonian or transition moments) are constructed from tensor products of elementary operators (*15, 16*). Rotational operators are given by tensor powers of the standard dimensionless angular moment operators referenced to molecule-fixed axes. Vibrational operators are given by tensor products of creation and annihilation elementary operators associated with the four normal modes of the molecule. Rovibrational Hamiltonian operators are then obtained from totally symmetric and Hermitian tensor products of the previous operators. As in Ref. (*9*) the effective rovibrational Hamiltonian was developed through the fourth order of approximation.

The dipolar transition moment is similarly expressed in tensorial form. It is partially transformed according to the polyad pattern of the CH_4 molecule. In the present work, the Pentad–G.S. transition moment operators are denoted by $\Omega(K,$

0022-2852/00 $35.00

TABLE 1
Transition Moment Parameters

order	Nomenclature			operator type	$^{12}CH_4$		$^{13}CH_4$	
		rotation	vibration		Hilico et al. (1994)	present work	present work	
0	μ_3	0(0,0A$_1$)	0010 F$_2$	a_3	-9.167(16)	- 9.2185(45)	-9.210(15)	10^{-2}
1	μ_{24}	0(0,0A$_1$)	0101 F$_2$	$a_2 \times a_4$	7.182(48)	7.924(20)	8.188(65)	10^{-3}
1	μ_{44}	0(0,0A$_1$)	0002 F$_2$	$a_4 \times a_4$	2.0461(26)	2.0268(11)	1.9691(34)	10^{-2}
1	μ'_3	1(1,0F$_1$)	0010 F$_2$	$J \times a_3$	2.409(99)	2.703(30)	2.36(11)	10^{-4}
2		1(1,0F$_1$)	0200 E	$J \times a_2 \times a_2$	-2.47(17)	-4.43(46)	36.8(1.8)	10^{-6}
2		1(1,0F$_1$)	0101 F$_1$	$J \times a_2 \times a_4$	-2.28(20)	-3.273(77)	-0.46(42)	10^{-5}
2	μ'_{24}	1(1,0F$_1$)	0101 F$_2$	$J \times a_2 \times a_4$	-4.83(31)	-3.83(10)	-7.64(42)	10^{-5}
2		1(1,0F$_1$)	0002 E	$J \times a_4 \times a_4$	5.395(92)	5.253(47)	4.07(28)	10^{-5}
2	μ'_{44}	1(1,0F$_1$)	0002 F$_2$	$J \times a_4 \times a_4$	-8.73(18)	-9.280(95)	-4.53(33)	10^{-5}
2		2(2,0F$_2$)	1000 A$_1$	$J^2 \times a_1$	0.723(91)	1.110(38)	4.83(74)	10^{-6}
2		2(0,0A$_1$)	0010 F$_2$	$J^2 \times a_3$	0.0 *	1.06(19)	-2.73(89)	10^{-6}
2		2(2,0E)	0010 F$_2$	$J^2 \times a_3$	4.02(25)	5.40(14)	3.23(48)	10^{-6}
2		2(2,0F$_2$)	0010 F$_2$	$J^2 \times a_3$	0.0 *	7.1(1.7)	23.8(6.6)	10^{-7}
3		2(2,0F$_2$)	0200 A$_1$	$J^2 \times a_2 \times a_2$		-2.56(14)	5.04(93)	10^{-7}
3		2(2,0F$_2$)	0200 E	$J^2 \times a_2 \times a_2$		5.34(26)	-9.4(2.1)	10^{-7}
3		2(0,0A$_1$)	0101 F$_2$	$J^2 \times a_2 \times a_4$		6.84(74)	3.1(4.1)	10^{-7}
3		2(2,0E)	0101 F$_1$	$J^2 \times a_2 \times a_4$		1.255(59)	1.17(33)	10^{-6}
3		2(2,0E)	0101 F$_2$	$J^2 \times a_2 \times a_4$		-1.333(62)	-0.78(35)	10^{-6}
3		2(2,0F$_2$)	0101 F$_1$	$J^2 \times a_2 \times a_4$		-1.91(40)	0.0 *	10^{-7}
3		2(2,0F$_2$)	0101 F$_2$	$J^2 \times a_2 \times a_4$		3.01(62)	0.0 *	10^{-7}
3		2(0,0A$_1$)	0002 F$_2$	$J^2 \times a_4 \times a_4$		-5.63(57)	11.7(2.6)	10^{-7}
3		2(2,0E)	0002 F$_2$	$J^2 \times a_4 \times a_4$		9.65(59)	7.5(3.4)	10^{-7}
3		2(2,0F$_2$)	0002 A$_1$	$J^2 \times a_4 \times a_4$		3.15(26)	7.8(5.9)	10^{-7}
3		2(2,0F$_2$)	0002 E	$J^2 \times a_4 \times a_4$		2.37(40)	-4.1(2.4)	10^{-7}
3		2(2,0F$_2$)	0002 F$_2$	$J^2 \times a_4 \times a_4$		-3.95(51)	-10.6(3.3)	10^{-7}

Parameters are given in Debye. Uncertainties in parentheses are one standard deviation in units of the last digits quoted. J designates the angular momentum tensor, a_s the annihilation operator for the normal mode s.

Γ_r) $n_1\ n_2\ n_3\ n_4\ \Gamma_v$. The corresponding operators are formally expressed as

$$(R^{\Omega(K,\Gamma_r)} \times (a_1^{n_1} \times a_2^{n_2} \times a_3^{n_3} \times a_4^{n_4})^{(\Gamma_v)})^{(F_2)}, \qquad [1]$$

where Ω is the degree in elementary components J_α, K the tensor rank relative to the space rotation group $O(3)$, Γ_r and Γ_v designate the symmetry in the T_d point group of the rotational and vibrational operators, respectively. The indices $n_1\ n_2\ n_3\ n_4$ are the powers of the annihilation operators associated with the four vibrational modes. The order of magnitude classification is defined by the sum $\Omega + n_1 + n_2 + n_3 + n_4 - 1$. Details concerning the operator symmetrization and classification are given in Ref. (*17*).

The Pentad system contains three F_2 sublevels belonging to ν_3, $\nu_2 + \nu_4$, and $2\nu_4$. Therefore, the dipole-moment expansion contains three purely vibrational terms classically denoted μ_3, μ_{24}, and μ_{44}. J-dependent terms of vibrational symmetry F_2 denoted by μ'_3, μ'_{24}, and μ'_{44} are usually interpreted as correction terms analogous to the Herman–Wallis terms in the theory of diatomics. However, for tetrahedral molecules, a complete expansion to the first order of approximation contains three extra J-dependent terms. In the present work, the effective dipole moment was developed through the third order of approximation (Table 1). The corresponding number of symmetry-allowed terms is 29 including J-dependent terms up to the third power. In fact, the four J^3-type operators were not statistically determinable in our study.

It should be emphasized that due to ambiguities among effective Hamiltonians of polyatomic molecules, the values of some of the dipole-moment parameters depend on the reduction chosen for the calculation of energies, i.e., on the implicit choice of the orientation of the eigenvectors (*18, 19*). It means that the set of fitted values would lose their meaning if separated from the set of Hamiltonian parameters from which the eigenvectors and eigenvalues are calculated.

3. EXPERIMENTS

Intensity measurements from two sources have been used in the present work: (i) data from laser spectrometry including allowed (strong) lines of the ν_3 band already reported in (*10, 4, 11, 12*); (ii) new measurements from Fourier transform spectra recorded at KPNO covering all the bands with a dynamic range

TABLE 2
Conditions of the Experimental FTS Measurements

Normal sample $^{12}CH_4$			Enriched $^{13}CH_4$		
Pres. Torr	Path m	Temp. K	Pres. Torr	Path m	Temp. K
0.97	0.05	296.1	0.97	0.25	295.7
0.49	0.25	295.9	0.97	0.25	295.7
1.00	0.25	296.3	2.29	0.25	295.4
4.68	0.25	295.2	5.93	0.25	295.9
5.97	1.50	296.3	2.98	1.50	295.4
0.41	1.50	297.3	8.83	1.50	296.2
2.02	1.50	297.3			
10.05	1.50	297.3			
1.90	2.40	298.4			
8.00	2.40	298.9			
3.44	25.00	291.0			
3.44	73.00	291.0			
3.44	193.00	291.0			
3.44	433.00	291.0			

extending from 7×10^{-6} to 8 cm^{-2} atm^{-1}, i.e., including numerous weak and perturbation-allowed lines. These new empirical intensities were selective remeasurements to improve the precision and accuracy of the values from Toth *et al.* (*8*) which had been used, along with those of Dang-Nhu *et al.* (*4*), by Hilico *et al.* (*9*) to model Pentad intensities with a reported accuracy of 8%. For this new effort, 14 spectra of $^{12}CH_4$ and six of isotopically enriched $^{13}CH_4$ were recorded at room temperature. The gas conditions are shown in Table 2. These were obtained at a spectral resolution of 0.012 cm^{-1} using matched InSb detectors and a globar source to record a band pass from 1800 to 5200 cm^{-1} with integration times of 60–70 min per spectrum. Uncertainty in the recorded temperatures is 1.5 K. Line intensities were retrieved using least-squares curve fitting (*20*). Observed values were obtained by averaging retrievals from three to eight different spectra. The rms agreement of the observed intensity was taken as the initial indication of precision. Measurements were eliminated from consideration if the rms was greater than 15% or if overlapped by other transitions.

The recent laser measurements (*11*, *12*) were intended to provide accurate linewidths rather than absolute intensities. To make the available data consistent, we refit the *Q* branch for integrated line intensities and applied very small scaling factors with respect to the measurements published in Ref. (*4*) (see Table 3).

While the laser data are essentially restricted to strong ν_3 allowed lines, the FTS data cover several orders of magnitude and all the bands of the pentad system as illustrated in Figs. 1 and 2. Both isotopes $^{12}CH_4$ and $^{13}CH_4$ have been considered while the majority of data are concerned with the main $^{12}CH_4$ isotope. Attention was paid to the consistency for both positions and intensities since line positions are de facto involved in the profile-fitting procedure used to measure intensities.

We focused on a set of positions (mainly ν_3) obtained by curve-fitting a spectrum recorded at 0.0117 cm^{-1} with a gas pressure of 0.2 Torr. The calibration standards were the *P* branch of ν_3 (Brault, private communication) based on the P7 line (*21*) at 2947.912106 cm^{-1} and the 2–0 band of CO (*22*). The overall absolute accuracy of the positions is thought to be 0.0002 cm^{-1} or better for unblended features. These reference wavenumbers were compared to the corresponding wavenumbers fitted in Ref. (*9*), and a significant systematic offset of 0.0005 cm^{-1} was observed. Since transitions from different sources were simultaneously fitted in Ref. (*9*), we repeated the global fit after applying a uniform correction of 0.0005 cm^{-1} to the 4559 fitted wavenumbers of the transitions from the ground

TABLE 3
Scaling Factors, Weights, and Global Statistics of the Simultaneous Fits

Data Origin	Scaling factor	Nb lines	*J* max	Temperature	Precision used for weighting	χ^2	Unweighted R.M.S.	Unweighted Mean
				$^{12}CH_4$				
Present FTS data		2141	21	296	3.0%	0.992	2.90%	- 0.01%
Pine (1997)	0.9965	98	11	296	1.5%	0.738	1.05%	0.27%
Pine (1992)	0.9975	66	13	296	1.5%	1.012	1.65%	0.45%
Pine (1976)	1.0050	125	11	295	1.5%	0.638	0.91%	0.32%
Dang-Nhu et al. (1979)	1.0000	30	7	294.7	1.5%	0.597	0.86%	0.33%
All $^{12}CH_4$		2460				0.972	2.77%	0.04%
				$^{13}CH_4$				
Present FTS data		482	15	296	3.0%	1.296	3.83%	0.36%
Dang-Nhu et al. (1979)		27	7	295	1.5%	0.973	1.49%	-0.14%
All $^{13}CH_4$		509				1.311	3.74%	0.33%

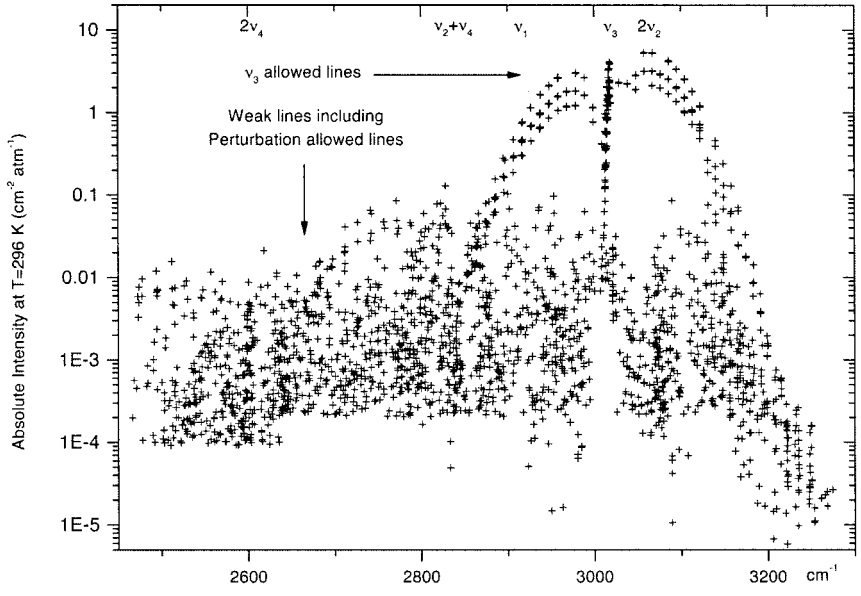

FIG. 1. Coverage of the intensity measurements for $^{12}CH_4$.

state to the Pentad upper states. The other types of transition (Pentad–Dyad infrared and Pentad–G.S. Raman) were kept unchanged. The statistical results of the global fit of positions are reported in Table 4. The precisions of the measured positions and intensities can be judged by the obs − calc values quoted in Table 5. Lines that are closer than 0.02 cm^{-1} probably have worse precisions than the well-isolated lines. We note that the observed value of the P7 line is 2947.91199 cm^{-1} rather than the expected value, and this is taken as an indication of the absolute accuracy.

After correction, the mean discrepancies of the three independent sets of data were found reasonably consistent within the interval -0.00019 to $+0.00026$ cm^{-1}. A statistical analysis of the obs − calc residuals of the ν_3 transitions of the reference list was also performed in order to compare the relative precision of the wavenumbers used in Ref. (*9*) and the newly calibrated measurements. The root-mean-squares from the 287 selected lines were almost equal for both sets indicating that no significant improvement of the relative precision of positions could be expected by using new wavenumbers. The methane

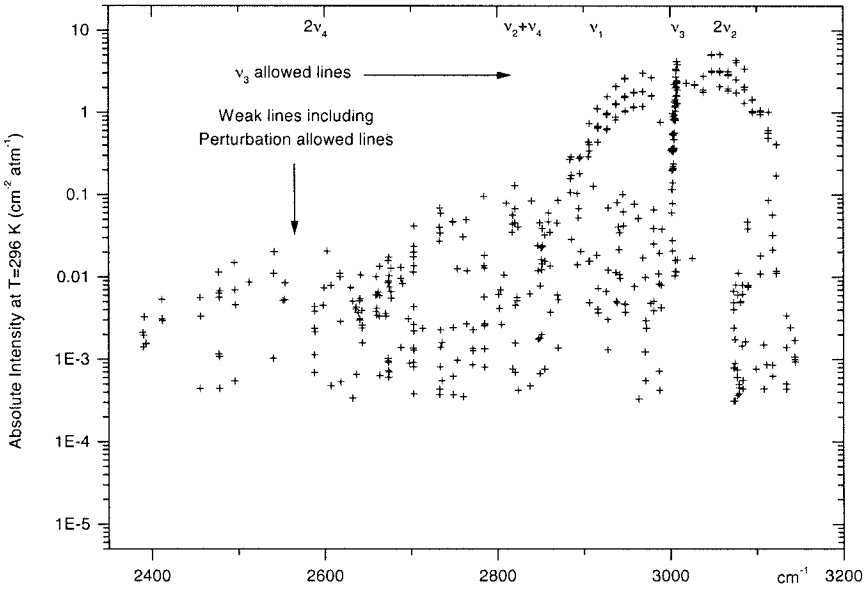

FIG. 2. Coverage of the intensity measurements for $^{13}CH_4$.

TABLE 4
Frequency Calibration

Data set	Nb lines	J max	mean 10^{-3} cm^{-1}	R.M.S. cm^{-1}
Fitted Pentad IR	4559	18	0.075	1.84
Fitted Pentad–Dyad IR	1115	12	0.26	0.80
Fitted Pentad Raman	146	17	-0.19	1.67
All fitted data	6122	18	0.09	1.67
Reference list	287	16	-0.09	1.28

line parameters proposed as secondary standards are listed in Table 5. As expected the 0.0005 cm^{-1} offset correction to the selected positions had negligible effect on the eigenvectors with only the band centers being significantly modified with respect to the study of Ref. (*9*).

4. ANALYSIS

The analysis of the newly measured FTS intensities was achieved by simultaneously fitting all data available (including previously reported laser data) and by comparing interactively various experimental scans to the corresponding synthetic spectra (including the known isotopic contributions).

A careful selection of data was achieved by rejecting blended lines. The resulting sets of data were fitted using a global nonlinear weighted least-squares method to minimize the dimensionless quantity

$$S^2 = \sum_i p_i e_i^2 = \sum_i \frac{(S_i^{\text{obs}} - S_i^{\text{calc}})^2}{(\sigma_i S_i^{\text{calc}})^2}, \qquad [2]$$

where σ_i designates the relative experimental precision of the ith data. The corresponding weight is $p_i = 1/(\sigma_i S_i^{\text{calc}})^2$.

Two different weighting methods were used and tested.

In a first step, the individual precisions were determined from the standard deviations derived from profile fitting with a threshold set to 1.5% to account for the estimated absolute uncertainty (pressure, temperature, etc.).

The χ^2 values for the various sets of data obtained from the simultaneous fit ranged from 0.47 to 1.0% indicating that the model accuracy was at least comparable to the experimental precision.

In a second step, we used the global standard deviations obtained from the fit to estimate the experimental precision assuming a uniform value for each set.

The above two fits were in fact very close to each other regarding both parameter values and intensity predictions (differences generally much smaller than the precisions). For simplicity, in the final fit we used uniform values for the precisions: 3% for all FTS data and 1.5% for all laser data.

5. RESULTS

The pentad band system includes the strong allowed fundamental band ν_3, weaker harmonic and combination bands involving forbidden transitions, and the forbidden totally symmetric fundamental band ν_1. However, due to perturbations, all the vibrational sublevels were observed and covered by numerous measurements. They were fitted with a similar precision. The global statistical results of the simultaneous fits are summarized in Table 3. For all isotopes the χ^2 value is close to unity indicating that the experimental precision is correctly estimated and that the model accuracy is consistent. The detailed statistics reported in Table 6 show the consistency of the various sets of data fitted simultaneously. Finally statistics by bands are given in Tables 7 and 8 for each isotope. It can be seen that the quality of the rms agreement does not vary significantly with increasing J. The accuracy achieved on the weaker and forbidden bands is also quite satisfactory.

The model used in Ref. (*9*), in which 11 parameters (through the second order of approximation) were adjusted, was first tested on the new data. A smaller standard deviation was achieved confirming that a better precision of the experimental data was absolutely necessary. However, thanks to the flexibility of the tensorial formalism, higher order terms could be tested readily and our best fit was obtained using an expansion up to the third order of approximation. Finally, 25 effective dipole moment parameters could be determined for $^{12}CH_4$ (Table 1). The standard deviations of the parameters are generally smaller than in the previous study.

For $^{13}CH_4$ the same expansion was considered although two parameters were fixed to zero because they were found statistically undeterminable, probably due to the smaller number of data generally restricted to lower J values.

Some of the higher order parameters have quite different values for $^{12}CH_4$ and $^{13}CH_4$ (see for instance the $2\nu_2$ J-dependent correction). The main reason is that effective dipole-moment parameters are essentially dependent of the reduction chosen for the effective Hamiltonian (*18*, *19*). In the present work, the reduced forms of the effective Hamiltonians for $^{12}CH_4$ and $^{13}CH_4$ are different because they are obtained from independent studies (*9*, *13*) for which the number and distribution of the available positions also varied.

The relatively large number of dipole-moment parameters fitted in the present work reflects the complexity of the vibration–rotation interactions and confirms the efficiency of the tensorial formalism while the semiempirical Herman–Wallis-type formulation (with six adjustable parameters) is clearly inadequate at this level of accuracy. The correspondence between tensorial and classical lower order parameters is not explicitly given since, as mentioned before, the individual values of the parameters are meaningful only when the full set of parameters is considered. Furthermore the values and physical meaning of the higher order terms can be precisely assessed only in connection with the study of the corresponding

TABLE 5

ν_3 Band of $^{12}CH_4$: Secondary Standards

	Position	a	Intensity	b	c		Position	a	Intensity	b	c
$P13, F_1, 4$	2884.38616	-0.51	0.091			$P7, F_1, 2$	2947.66788	-0.01	1.264		-0.3
$P13, E, 2$	2884.44841	-0.17	0.060	2.0		$P7, E, 1$	2947.81090	0.05	0.839	1.1	0.4
$P13, F_2, 3$	2884.51134	-0.83	0.090	2.4		$P7, F_2, 2$	2947.91199	-0.01	1.249	-0.7	0.0
$P13, A_2, 1$	2885.08881	-0.63	0.148			$P7, A_2, 1$	2948.10787	0.02	2.071	-1.0	-0.6
$P13, F_2, 2$	2885.23462	0.21	0.088	0.7		$P7, F_2, 1$	2948.42131	-0.02	1.267		0.1
$P13, F_1, 3$	2885.35151	-0.07	0.088	-0.1		$P7, F_1, 1$	2948.47410	0.09	1.272	0.6	0.6
$P13, A_1, 1$	2885.76109	-0.71	0.149	3.3		$P6, A_1, 1$	2958.01720	0.00	2.593	-1.3	0.2
$P13, F_1, 2$	2885.84717	-0.97	0.089	1.9		$P6, F_1, 1$	2958.12000	0.02	1.546	-1.0	0.7
$P13, E, 1$	2885.87733	-1.05	0.059	2.6		$P6, F_2, 2$	2958.23287	-0.01	1.533	-0.9	0.9
$P13, F_2, 1$	2886.60518	-0.08	0.091			$P6, A_2, 1$	2958.53624	-0.07	2.603	-2.1	-0.2
$P13, F_1, 1$	2886.61317	0.56	0.091	3.5		$P6, F_2, 1$	2958.65064	-0.13	1.554		0.9
$P12, A_1, 2$	2894.99631	0.02	0.275	0.8		$P6, E, 1$	2958.68255	0.06	1.039	2.1	0.8
$P12, F_1, 3$	2895.05590	-0.27	0.164	1.2		$P5, F_1, 2$	2968.40321	-0.03	1.745		0.0
$P12, F_2, 3$	2895.12884	-0.21	0.163	0.8		$P5, E, 1$	2968.47349	-0.13	1.156	1.2	0.0
$P12, A_2, 1$	2895.23336	-0.26	0.273			$P5, F_2, 1$	2968.73616	-0.04	1.757	-0.4	0.6
$P12, F_2, 2$	2895.75776	-0.08	0.159			$P5, F_1, 1$	2968.85509	-0.12	1.754	-0.8	0.5
$P12, E, 2$	2895.82690	-0.33	0.107	-0.7		$P4, F_2, 1$	2978.65036	-0.15	1.776		0.5
$P12, F_1, 2$	2896.20251	-0.41	0.161	0.1		$P4, E, 1$	2978.84805	-0.09	1.192	0.7	0.1
$P12, F_2, 1$	2896.29970	-0.39	0.161			$P4, F_1, 1$	2978.91991	0.00	1.785	-0.3	0.4
$P12, E, 1$	2896.97511	0.04	0.110			$P4, A_1, 1$	2979.01119	-0.14	2.982	-1.4	0.4
$P12, F_1, 1$	2896.98025	-0.17	0.165			$P3, A_2, 1$	2988.79521	-0.11	2.646	-1.0	-0.5
$P12, A_1, 1$	2896.99037	-0.09	0.275	-4.3		$P3, F_2, 1$	2988.93233	-0.25	1.583	-0.2	-0.2
$P11, F_1, 3$	2905.63369	-0.04	0.280			$P3, F_1, 1$	2989.03346	-0.05	1.587		0.4
$P11, E, 2$	2905.69756	-0.05	0.185			$P2, F_2, 1$	2998.99389	-0.15	1.125		0.5
$P11, F_2, 3$	2905.81367	-0.16	0.278			$P2, E, 1$	2999.06026	-0.17	0.750		0.8
$P11, F_1, 2$	2906.28237	-0.19	0.273			$Q13, F_2, 1$	3008.84756	1.15	0.125		
$P11, E, 1$	2906.58859	-0.37	0.182	1.5		$Q13, F_1, 1$	3008.85083	4.01	0.125		
$P11, F_2, 2$	2906.64766	-0.06	0.274	1.9		$P1, F_1, 1$	3009.01127	-0.09	0.420		-3.1
$P11, A_2, 1$	2906.73483	-0.15	0.459	1.7		$Q12, F_1, 1$	3010.17738	0.99	0.220		
$P11, F_2, 1$	2907.32118	-0.22	0.281	4.0		$Q12, A_1, 1$	3010.17746	1.46	0.367		
$P11, F_1, 1$	2907.33607	-0.11	0.281	4.6		$Q12, E, 1$	3010.17984	3.28	0.146		
$P10, F_2, 3$	2916.20137	-0.22	0.449	-0.2	0.8	$Q14, A_1, 1$	3010.67042	-1.15	0.105		
$P10, E, 2$	2916.30165	-0.16	0.298		1.1	$Q14, F_1, 2$	3010.75205	0.04	0.062		
$P10, F_1, 2$	2916.39613	-0.17	0.442		0.5	$Q14, E, 2$	3010.80430	-0.44	0.042		
$P10, A_1, 1$	2916.75382	0.04	0.730		0.8	$Q15, A_2, 2$	3010.87885	-0.37	0.053		
$P10, F_1, 1$	2916.96607	-0.14	0.437	1.0	0.8	$Q13, E, 1$	3010.88374	0.04	0.077		
$P10, F_2, 2$	2917.06617	0.08	0.441		1.0	$Q13, F_1, 2$	3010.89354	0.51	0.115		
$P10, A_2, 1$	2917.62881	-0.27	0.752		1.2	$Q13, A_1, 1$	3010.91172	0.14	0.191		
$P10, F_2, 1$	2917.65113	-1.41	0.451		3.7	$Q14, F_2, 3$	3011.24103	-0.63	0.064		
$P10, E, 1$	2917.66115	-1.65	0.300		-1.4	$Q11, F_1, 1$	3011.43311	0.73	0.368		
$P9, A_2, 1$	2926.70021	0.07	1.132	0.8	0.0	$Q11, F_2, 1$	3011.43622	1.64	0.368		
$P9, F_2, 2$	2926.78278	-0.11	0.676		0.2	$Q13, F_2, 2$	3011.92974	-0.16	0.117		
$P9, F_1, 3$	2926.88493	-0.09	0.669	-0.4	0.3	$Q12, F_2, 1$	3012.02940	-0.16	0.206		
$P9, A_1, 1$	2927.07606	-0.03	1.122	1.7	0.8	$Q12, F_1, 2$	3012.06281	-0.09	0.205		
$P9, F_1, 2$	2927.37259	0.03	0.661	1.1	0.5	$Q13, A_2, 1$	3012.22924	-0.33	0.202	0.8	
$P9, E, 1$	2927.42908	0.00	0.444	0.8	1.2	$Q13, F_2, 3$	3012.50366	0.48	0.117		1.7
$P9, F_2, 1$	2927.93203	-0.02	0.680	2.0	1.1	$Q13, E, 2$	3012.60275	1.59	0.079		4.6
$P9, F_1, 1$	2927.96354	0.09	0.680	1.9	1.1	$Q10, E, 1$	3012.61293	0.87	0.387		-1.3
$P8, F_2, 2$	2937.23458	0.04	0.958	0.7	-0.7	$Q10, F_2, 1$	3012.61566	0.66	0.581		-1.1
$P8, E, 2$	2937.30818	0.11	0.634	-1.0	-0.6	$Q10, A_2, 1$	3012.62122	0.37	0.968		-1.1
$P8, F_1, 2$	2937.49478	-0.14	0.950	0.9	0.5	$Q13, F_1, 4$	3012.71016	0.10	0.120	0.8	4.6
$P8, F_2, 1$	2937.76721	0.09	0.940	1.6	-0.2	$Q7, A_2, 1$	3012.79691	1.05	0.056		
$P8, E, 1$	2938.19249	-0.03	0.641	2.0	0.8	$Q12, E, 2$	3012.85245	-0.49	0.141	0.9	6.0
$P8, F_1, 1$	2938.21524	-0.05	0.962	2.4	0.3	$Q12, F_2, 2$	3012.91616	0.02	0.210		1.4
$P8, A_1, 1$	2938.25175	0.05	1.606	-0.4	0.1	$Q11, A_2, 1$	3013.07817	-0.07	0.585	-0.4	0.4

Position: measured values from FTS spectra with an absolute accuracy of 0.0002 cm^{-1}.

Intensities: predicted values in cm^{-2} atm^{-1} in natural abundance at 296 K using the parameters obtained from the simultaneous fit of FTS and laser data within the Pentad scheme.

The absolute accuracy is estimated to 2%.

a : *Obs* − *Calc* Position residual of FTS data (in $10^{-3}cm^{-1}$)

b : *Obs* − *Calc* Intensity residual of fitted FTS data (in %)

c : *Obs* − *Calc* Intensity residual of re-analyzed laser data of Refs. [11, 12] (in %)

TABLE 5—*Continued*

	Position	a	Intensity	b	c		Position	a	Intensity	b	c
$Q11, F_2, 2$	3013.12694	-0.21	0.347	-1.2	-1.2	$R4, F_2, 1$	3067.16419	0.45	3.138		-0.1
$Q11, E, 1$	3013.15577	0.15	0.230	-5.0	0.3	$R4, E, 1$	3067.23439	0.44	2.077	0.2	0.3
$Q12, A_2, 1$	3013.16698	-0.07	0.348		0.9	$R4, F_1, 1$	3067.26108	0.46	3.117		0.1
$Q12, F_2, 3$	3013.40778	0.04	0.210		2.3	$R4, A_1, 1$	3067.30009	0.32	5.205		-0.7
$Q12, F_1, 3$	3013.51150	0.10	0.213	1.2	4.6	$R5, F_1, 2$	3076.54950	0.31	2.906	-0.6	-0.8
$Q12, A_1, 2$	3013.59264	0.11	0.359	0.1	2.0	$R5, E, 1$	3076.56876	0.29	1.936		0.7
$Q9, F_1, 1$	3013.71097	0.15	0.868	-1.2	-2.0	$R5, F_2, 1$	3076.67695	0.45	2.871	-0.4	0.0
$Q9, F_2, 1$	3013.72356	0.09	0.865	-0.2	-2.2	$R5, F_1, 1$	3076.72521	0.47	2.881	-2.1	-0.4
$Q11, F_1, 2$	3013.80651	0.00	0.360	0.7	1.4	$R6, A_1, 1$	3085.83210	0.30	4.173		0.5
$Q11, F_2, 3$	3014.06040	-0.20	0.353		0.8	$R6, F_1, 1$	3085.86064	0.39	2.497	0.5	0.3
$Q10, F_2, 2$	3014.09532	-0.21	0.559		3.5	$R6, F_2, 2$	3085.89351	0.37	2.491	0.0	0.7
$Q10, F_1, 1$	3014.17172	-0.16	0.548		1.1	$R6, A_2, 1$	3086.03071	0.51	4.086		-0.1
$Q11, E, 2$	3014.27628	-0.23	0.239	1.2	1.6	$R6, F_2, 1$	3086.07146	0.16	2.461		1.3
$Q11, F_1, 3$	3014.34417	-0.02	0.362	0.9	1.1	$R6, E, 1$	3086.08552	0.05	1.643	0.5	1.3
$Q10, A_1, 1$	3014.64162	-0.10	0.957	-0.3	0.6	$R7, F_1, 2$	3095.06070	0.36	2.010	0.0	0.1
$Q8, A_1, 1$	3014.71163	0.03	2.041	-2.5	-1.4	$R7, E, 1$	3095.10383	0.12	1.333		0.0
$Q8, F_1, 1$	3014.73478	-0.01	1.216		-0.9	$R7, F_2, 2$	3095.13062	0.29	1.995		0.5
$Q8, E, 1$	3014.74706	0.04	0.808	4.4	-1.1	$R7, A_2, 1$	3095.17913	-0.02	3.329		-0.9
$Q10, F_1, 2$	3014.83842	-0.01	0.558	0.0	2.7	$R7, F_2, 1$	3095.35127	0.60	1.960	-1.0	0.3
$Q10, E, 2$	3014.94110	-0.28	0.380		2.7	$R7, F_1, 1$	3095.37108	0.31	1.965	0.3	-0.2
$Q9, E, 1$	3015.00143	-0.10	0.563		2.6	$R8, F_2, 2$	3104.20527	0.19	1.513	-0.2	-0.5
$Q9, F_1, 2$	3015.05054	-0.10	0.833		0.7	$R8, E, 2$	3104.22044	0.13	1.007	2.3	-0.1
$Q10, F_2, 3$	3015.09155	-0.16	0.577	0.2	1.2	$R8, F_1, 2$	3104.28392	0.37	1.498	0.8	-0.7
$Q9, A_1, 1$	3015.20315	-0.31	1.389	-0.6	0.2	$R8, F_2, 1$	3104.33642	-0.19	1.498	0.8	-0.3
$Q9, F_1, 3$	3015.59078	-0.25	0.846		0.4	$R8, E, 1$	3104.56888	0.25	0.976		0.7
$Q7, F_1, 1$	3015.64175	-0.08	1.613		1.0	$R8, F_1, 1$	3104.57458	-0.07	1.466		0.6
$Q7, F_2, 1$	3015.68246	-0.27	1.592		-0.3	$R8, A_1, 1$	3104.58533	-0.11	2.449	1.7	0.2
$Q9, F_2, 2$	3015.70617	-0.32	0.862	0.0	0.8	$R9, A_2, 1$	3113.26129	0.14	1.791		0.9
$Q9, A_2, 1$	3015.80475	-0.67	1.448	0.8	0.1	$R9, F_2, 2$	3113.27959	-0.01	1.070		0.4
$Q8, F_2, 1$	3015.81521	-0.74	1.199		-0.4	$R9, F_1, 3$	3113.30104	-0.25	1.033	0.7	0.3
$Q8, F_1, 2$	3015.98896	-0.43	1.187	1.1	0.5	$R9, A_1, 1$	3113.38038	0.98	1.764	0.3	0.1
$Q8, E, 2$	3016.30168	-0.30	0.810	0.3	-0.2	$R9, F_1, 2$	3113.41757	-0.10	1.021	1.8	0.7
$Q8, F_2, 2$	3016.36890	-0.44	1.221		-0.7	$R9, E, 1$	3113.42874	0.11	0.705	1.1	1.4
$Q6, E, 1$	3016.45808	-0.23	1.329	-2.2	0.3	$R10, F_2, 3$	3122.25766	0.01	0.709		1.3
$Q6, F_2, 1$	3016.48882	-0.52	1.975	0.8	0.3	$R10, E, 2$	3122.28446	-0.32	0.472	1.2	1.6
$Q7, A_2, 1$	3016.49775	-0.11	2.660		-0.6	$R10, F_1, 2$	3122.29580	-0.66	0.598	-0.5	0.3
$Q6, A_2, 1$	3016.56531	-0.36	3.273		-1.1	$R10, A_1, 1$	3122.33190	-0.93	1.185		1.7
$Q7, F_2, 2$	3016.64056	-0.23	1.580	-1.3	0.1	$R10, F_1, 2$	3122.36554	1.98	0.115		
$Q7, E, 1$	3016.73317	-0.27	1.061		0.9	$R10, F_1, 1$	3122.37078	-1.17	0.115		
$Q7, F_1, 2$	3016.93950	-0.43	1.619	0.1	-0.1	$R10, F_1, 1$	3122.43997	0.94	0.588		
$Q5, F_1, 1$	3017.16317	-0.23	2.288	-1.2	-1.1	$R10, F_2, 2$	3122.44376	-0.94	0.694		-6.4
$Q6, F_2, 2$	3017.22792	-0.38	1.967		0.0	$R10, F_2, 1$	3122.76216	-1.91	0.677		
$Q5, F_2, 1$	3017.26659	-0.37	2.264		0.6	$R10, A_2, 1$	3122.76449	1.59	1.137		1.5
$Q6, F_1, 1$	3017.34568	-0.47	1.987		0.3	$R10, E, 1$	3122.76539	0.88	0.452		
$Q6, A_1, 1$	3017.46689	-0.40	3.343		-0.5	$R11, F_1, 3$	3131.17090	-2.89	0.422		
$Q4, A_1, 1$	3017.71164	-0.25	4.050		-1.6	$R11, E, 2$	3131.17647	5.37	0.228		
$Q5, E, 1$	3017.76300	-0.29	1.522		-0.6	$R11, F_2, 3$	3131.20629	-0.88	0.266	-1.4	
$Q4, F_1, 1$	3017.81449	-0.57	2.406		-0.5	$R11, F_1, 2$	3131.24276	-1.47	0.427		
$Q5, F_1, 2$	3017.82490	-0.82	2.287		-0.5	$R11, E, 2$	3131.24769	4.41	0.072		
$Q4, E, 1$	3017.88564	-0.15	1.596	-0.4	-0.5	$R11, F_2, 3$	3131.26128	1.30	0.182		
$Q4, F_2, 1$	3018.20535	-0.23	2.419		-0.1	$R11, E, 1$	3131.32308	-1.46	0.071	5.5	
$Q3, F_1, 1$	3018.24206	-0.18	2.308		-0.3	$R11, F_2, 2$	3131.34729	-0.60	0.178	4.0	
$Q3, F_2, 1$	3018.35850	-0.19	2.294		-0.4	$R11, A_2, 1$	3131.38216	-1.24	0.733		
$Q3, A_2, 1$	3018.52868	-0.17	3.852		-1.0	$R11, E, 1$	3131.39637	-0.36	0.222		
$Q2, E, 1$	3018.59119	-0.16	1.282		-0.6	$R11, F_2, 2$	3131.40185	1.15	0.260		
$Q2, F_2, 1$	3018.65014	-0.07	1.917		-0.5	$R11, F_2, 1$	3131.73588	0.13	0.423		
$Q1, F_1, 1$	3018.82448	0.09	1.277		-0.9	$R11, F_1, 1$	3131.73720	0.74	0.417		
$R0, A_1, 1$	3028.75218	0.13	2.266	0.2	-1.4	$R12, F_2, 3$	3139.97164	-3.61	0.064		
$R1, F_1, 1$	3038.49843	0.24	2.179	0.0	-0.5	$R12, F_1, 3$	3139.97450	0.58	0.098		
$R2, F_2, 1$	3048.15074	-2.20	2.785	-1.2	0.0	$R12, A_1, 2$	3139.99209	-0.73	0.394	-1.8	
$R2, E, 1$	3048.16647	-2.24	1.857		0.4	$R12, F_1, 3$	3140.04353	0.16	0.156	-1.0	
$R3, A_2, 1$	3057.68734	0.35	5.187		0.0	$R12, F_2, 3$	3140.06454	-0.50	0.200		
$R3, F_2, 1$	3057.72640	0.34	3.103		0.5	$R12, F_2, 2$	3140.07149	0.95	0.222	-1.1	
$R3, F_1, 1$	3057.76069	0.40	3.102		0.6	$R12, E, 2$	3140.08478	-0.38	0.175		

TABLE 5—*Continued*

	Position	a	Intensity	b	c		Position	a	Intensity	b	c
$R12, A_2, 1$	3140.09026	1.73	0.445	1.4		$R13, F_1, 4$	3148.80985	0.80	0.115		
$R12, A_1, 2$	3140.13485	0.62	0.055	5.0		$R13, E, 2$	3148.81288	1.11	0.093		
$R12, F_1, 2$	3140.22144	0.34	0.158			$R13, F_1, 3$	3148.82023	-2.67	0.064		
$R12, F_2, 1$	3140.22216	-2.48	0.178			$R13, F_2, 2$	3148.82340	-2.01	0.129		
$R12, F_1, 2$	3140.29120	0.64	0.102	3.1		$R13, F_2, 3$	3148.82988	1.80	0.136		
$R12, F_2, 1$	3140.31598	1.54	0.043	3.9		$R13, F_1, 3$	3148.85783	-1.41	0.070	-4.9	
$R12, E, 1$	3140.62426	2.16	0.166			$R13, F_1, 2$	3148.99024	-1.08	0.082		
$R12, F_1, 1$	3140.62485	-0.69	0.237			$R13, E, 1$	3149.00140	0.37	0.090		
$R12, A_1, 1$	3140.63263	0.84	0.368			$R13, F_1, 2$	3149.02845	0.79	0.043		
$R13, A_2, 1$	3148.78505	-2.21	0.251			$R13, A_1, 1$	3149.04158	1.08	0.243	-2.6	

reduced forms of the effective Hamiltonian (*18, 19*). The main effect of higher order terms is to prevent the lower order terms from assuming anomalous values to account for higher order interactions.

As seen on the residuals plotted in Fig. 3 and in Tables 7 and 8, there are no apparent systematic deviations in the residuals as a function of the J quantum numbers or the vibrational bands.

Since several orders of magnitude are involved in the FTS data set, according to Eq. [2], the absolute weights of weak lines are much larger than the weights of strong lines. However, this weighting method is fully justified as shown by the residuals plotted versus the absolute intensities of the lines in Fig. 4. As a matter of fact, it can be seen that the residuals follow the opposite trend, i.e., on average, the relative discrepancies for strong lines are smaller than for weak lines.

Note that the precision of integrated bandstrength is principally determined by the precision of the stronger lines. In our case, it means that the precision of the whole pentad strength is closely related to the precision of the measurements of the ν_3 lines. It is interesting to compare the present integrated bandstrengths to previously published values. The quantities reported in Table 9 are calculated by summations over all transitions through $J = 30$ with an intensity threshold of 10^{-27} cm

TABLE 6
Statistical Comparison of the Different Sources of Data Simultaneously Fitted ($^{12}CH_4$)

	KPNO FTS data			Pine(1992) [11]			Pine(1976) [10]			Pine(1997) [12]			Dang Nhu(1979) [4]		
J	$n(J)$	$\sigma(J)$	$\mu(J)$	$n(J)$	$\sigma(J)$	$\mu(J)$	$n(J)$	$\sigma(J)$	$\mu(J)$	$n(J)$	$\sigma(J)$	$\mu(J)$	$n(J)$	$\sigma(J)$	$\mu(J)$
0	2	0.58	-0.58	0	0.00	0.00	1	2.09	-2.09	1	3.14	-3.14	0	0.00	0.00
1	15	5.78	-5.61	1	0.87	-0.87	4	1.30	1.28	3	0.81	0.57	1	0.61	-0.61
2	32	2.37	-0.10	2	0.55	-0.55	6	0.92	0.31	4	0.36	-0.09	1	0.08	0.08
3	63	1.74	-0.69	3	0.50	-0.45	8	0.76	0.55	6	0.33	0.28	2	0.29	0.22
4	86	1.57	0.14	4	0.61	-0.48	10	1.22	1.10	7	0.37	0.25	3	0.14	-0.13
5	134	2.63	-0.89	4	0.71	-0.45	14	0.61	0.29	10	0.73	0.63	10	0.42	0.05
6	173	2.71	-0.83	6	0.42	0.13	15	1.01	0.86	10	0.43	0.16	6	0.48	0.35
7	207	2.89	0.61	6	0.67	0.38	17	0.61	-0.04	13	0.65	0.11	7	1.78	1.55
8	209	3.05	-0.58	7	0.78	-0.57	19	0.74	0.30	14	0.86	0.72			
9	233	7.66	-5.26	8	1.76	0.43	18	1.00	-0.47	16	1.45	0.60			
10	202	4.10	2.21	9	2.08	0.99	11	1.18	0.51	8	1.08	0.97			
11	209	3.91	-3.43	7	1.13	0.71	2	0.75	-0.54	6	3.01	-0.19			
12	172	4.81	-1.11	6	4.23	3.74									
13	157	5.09	-2.52	3	4.09	3.89									
14	119	3.40	0.63												
15	53	4.60	0.49												
16	30	2.51	2.31												
17	17	2.44	2.38												
18	13	4.39	-2.74												
19	9	3.49	-2.28												
20	4	1.67	1.54												
21	2	2.56	-0.78												
	2141	2.90	-0.01	66	1.65	0.45	125	0.91	0.32	98	1.05	0.27	30	0.86	0.33

J : upper state quantum number ; $n(J)$: number of fitted lines ; $\sigma(J)$: unweighted root mean squares (in %) ; $\mu(J)$: unweighted mean (in %).

TABLE 7
Statistics of FTS Data by Subband versus J for $^{12}CH_4$

	ν_1		ν_3		$2\nu_2(A_1)$		$2\nu_2(E)$		$\nu_2+\nu_4(F_1)$		$\nu_2+\nu_4(F_2)$		$2\nu_4(A_1)$		$2\nu_4(E)$		$2\nu_4(F_2)$	
J	n	σ	n	σ	n	σ	n	σ	n	σ	n	σ	n	σ	n	σ	n	σ
0	–	–	–	–	–	–	–	–	–	–	1	0.8	–	–	–	–	1	0.6
1	–	–	1	0.2	–	–	4	5.8	2	3.1	3	1.1	–	–	2	1.3	3	0.9
2	–	–	3	0.4	1	1.0	2	1.5	5	4.6	8	0.9	–	–	4	1.8	9	2.6
3	–	–	10	1.3	2	3.4	3	2.0	8	1.7	15	4.9	2	0.5	5	1.2	18	0.9
4	–	–	11	4.5	1	2.1	10	3.3	11	0.8	18	1.6	3	1.8	11	2.5	21	0.6
5	–	–	22	2.3	3	3.2	9	2.9	23	3.6	24	4.0	3	2.4	13	1.9	37	2.6
6	–	–	32	5.0	7	3.3	15	3.3	33	5.0	28	2.5	2	0.6	21	1.4	35	3.1
7	–	–	30	4.6	12	4.6	18	6.0	36	3.8	47	2.5	5	2.2	21	1.7	38	2.5
8	–	–	32	3.2	9	1.4	31	3.8	46	3.6	40	4.3	1	0.8	25	2.6	25	2.2
9	–	–	37	4.1	15	3.6	35	8.2	50	3.2	42	2.9	3	0.1	15	1.2	36	3.4
10	–	–	42	6.2	9	3.1	37	4.2	46	2.6	29	2.0	2	1.9	14	2.0	23	3.6
11	–	–	44	3.8	5	6.8	39	3.4	46	4.9	35	1.3	3	0.6	15	6.3	22	2.4
12	8	4.1	32	3.5	3	3.1	32	5.0	29	3.9	41	2.6	–	–	10	2.8	17	1.4
13	6	3.1	39	4.2	3	6.6	29	5.1	38	3.7	29	2.5	–	–	4	2.3	9	1.7
14	3	6.2	30	6.5	2	5.1	22	3.1	28	4.3	26	2.5	1	7.4	2	1.8	5	1.7
15	–	–	20	7.7	–	–	7	4.7	12	5.2	14	2.9	–	–	–	–	–	–
16	–	–	22	4.6	–	–	1	2.4	4	5.6	3	1.4	–	–	–	–	–	–
17	1	2.2	15	2.1	–	–	1	3.2	–	–	–	–	–	–	–	–	–	–
18	–	–	13	4.4	–	–	–	–	–	–	–	–	–	–	–	–	–	–
19	–	–	9	3.5	–	–	–	–	–	–	–	–	–	–	–	–	–	–
20	–	–	4	1.7	–	–	–	–	–	–	–	–	–	–	–	–	–	–
21	–	–	2	2.6	–	–	–	–	–	–	–	–	–	–	–	–	–	–
Sum	18	4.8	450	2.8	72	5.6	295	4.6	417	4.1	403	2.7	25	3.3	162	3.1	299	2.6

J : upper state quantum number ; n : number of fitted lines ; σ : unweighted root mean squares (in %)

molecule^{-1} at $T = 296$ K in natural abundance. With respect to Ref. (*9*), the bandstrengths are corrected by values ranging from -5.2% ($2\nu_4$) to $+6.0\%$ (ν_1). In our calculations, the vibrational labels are based on the eigenvector components so that apparent transfers of intensity from one vibrational state to another can be simply induced by small changes in the eigenvector coefficients, especially when the forbidden ν_1 band is involved.

The ν_3 band is predicted $+2\%$ above the previous estimation while the correction for the whole polyad is $+1.6\%$. The

TABLE 8
Statistics of FTS Data by Subband versus J for $^{13}CH_4$

	ν_1		ν_3		$2\nu_2(A_1)$		$2\nu_2(E)$		$\nu_2+\nu_4(F_1)$		$\nu_2+\nu_4(F_2)$		$2\nu_4(A_1)$		$2\nu_4(E)$		$2\nu_4(F_2)$	
J	n	σ	n	σ	n	σ	n	σ	n	σ	n	σ	n	σ	n	σ	n	σ
0	–	–	–	–	–	–	–	–	–	–	–	–	–	–	–	–	1	0.3
1	–	–	3	1.3	–	–	–	–	2	3.3	2	1.0	–	–	–	–	2	0.4
2	–	–	7	1.3	–	–	–	–	1	1.4	3	1.4	–	–	–	–	5	1.1
3	–	–	7	1.7	–	–	1	2.3	4	0.6	8	10.9	–	–	1	1.8	7	0.9
4	–	–	11	1.3	2	2.1	1	8.4	7	1.8	14	1.3	–	–	4	1.4	3	0.5
5	–	–	17	7.8	–	–	–	–	2	4.9	17	8.5	–	–	2	0.5	12	4.4
6	–	–	20	6.6	–	–	5	9.8	8	6.6	2	0.2	–	–	6	3.5	8	4.0
7	–	–	19	2.4	3	4.7	4	1.1	9	8.1	20	7.5	–	–	4	3.9	2	1.0
8	–	–	26	6.9	1	2.0	7	5.3	5	3.7	10	4.6	–	–	–	–	4	0.8
9	–	–	23	4.3	2	0.9	6	5.5	6	13.7	15	11.5	–	–	2	3.4	9	3.1
10	–	–	17	2.5	–	–	4	2.8	6	2.3	6	0.7	–	–	1	2.0	–	–
11	–	–	24	3.2	–	–	2	6.7	7	6.7	10	4.0	–	–	–	–	1	0.2
12	–	–	14	2.2	–	–	–	–	3	6.9	1	5.3	–	–	–	–	1	2.1
13	–	–	8	3.5	–	–	–	–	–	–	–	–	–	–	–	–	–	–
14	–	–	4	4.2	–	–	–	–	–	–	1	1.1	–	–	–	–	–	–
Sum	–	–	200	3.7	8	3.7	30	5.3	60	7.7	109	8.0	–	–	20	3.4	55	3.1

J : upper state quantum number ; n : number of fitted lines ; σ : unweighted root mean squares (in %)

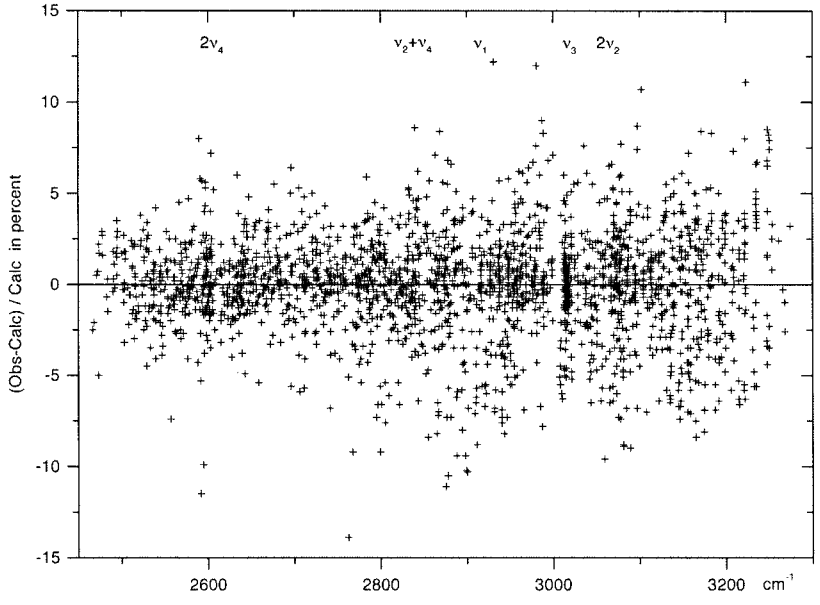

FIG. 3. Residuals $^{12}CH_4$ (all data fitted).

correction is principally explained by the fact that in earlier studies (*5, 9*) the data extracted from the AFGL compilation (*7*) were not corrected for isotopic abundance. Note that, at the level of precision of 10%, the consequences were almost negligible.

The accuracies of the pentad intensities depend on the band. For the four weaker bands, line intensities have been measured only twice, the first in the studies described by Toth *et al.* (*8*) and the second in the present effort. The present results are considered to be better because of the quality of the spectra (grating at 0.02 cm^{-1} resolution and 100:1 signal-to-noise versus FTS at 0.012 cm^{-1} resolution and 900:1 signal-to-noise) and the data reduction techniques (hand measurements with a planimeter versus least-squares curve fitting). For the main isotope, the differences of up to 6% between the old and new bandstrengths shown in Table 9 are thought to indicate the precision and accuracy of the old measurements for the weaker bands. In contrast, for the ν_3 fundamental, the new FTS measurements and the laser data agree within 0.5%. Furthermore, the intensity sum of the pentads for the two isotopes in Table

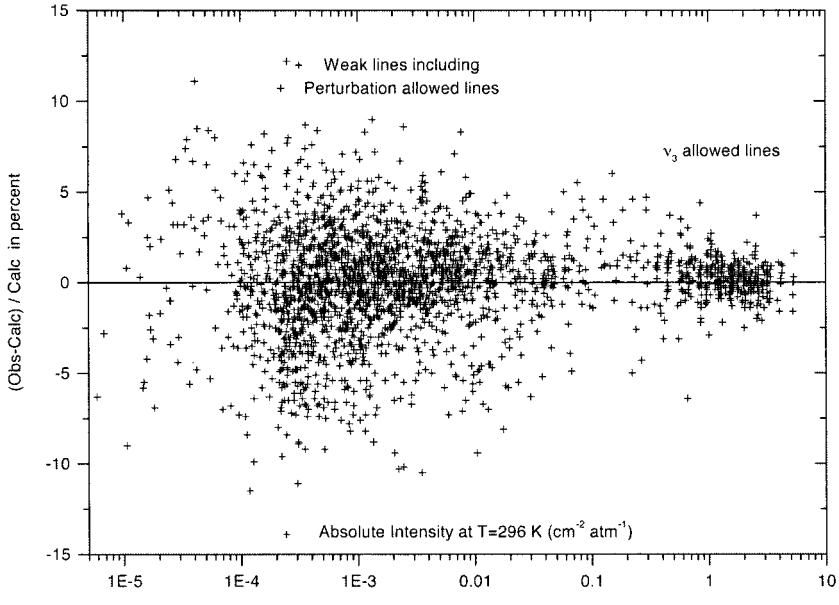

FIG. 4. Residuals versus absolute intensity $^{12}CH_4$.

TABLE 9
Calculated Bandstrengths of Methane

Band	$^{12}CH_4$ Hilico et al. (1994)		$^{12}CH_4$ Present Work		Variation %	$^{13}CH_4$	
	Nb lines	Summation	Nb lines	Summation		Nb lines	Summation
ν_3	6159	$1.056\ 10^{-17}$	4706	$1.076\ 10^{-17}$	+2.0%	3588	$1.247\ 10^{-19}$
ν_1	1104	$1.576\ 10^{-21}$	989	$1.671\ 10^{-21}$	+6.0%	448	$1.247\ 10^{-23}$
$2\nu_2$	3576	$3.280\ 10^{-20}$	3428	$3.174\ 10^{-20}$	-3.2%	1607	$2.518\ 10^{-22}$
$\nu_2 + \nu_4$	9241	$3.913\ 10^{-19}$	8376	$3.720\ 10^{-19}$	-4.9%	4962	$4.494\ 10^{-21}$
$2\nu_4$	6735	$5.795\ 10^{-20}$	6374	$5.488\ 10^{-20}$	-5.2%	3160	$6.390\ 10^{-22}$
Pentad	26815	$1.104\ 10^{-17}$	23873	$1.122\ 10^{-17}$	+1.6%	13765	$1.301\ 10^{-19}$

Values are given in cm molecule $^{-1}$ in natural abundance at 296 K

9 agree within 1% of the average of integrated intensities reported by 12 studies listed in a review by Kim (*23*). It is therefore expected that future intensity measurements of the ν_3 allowed lines will confirm an absolute accuracy of at least 2% for the present work.

The statistical uncertainties of the parameters given in Table 1 do not reflect possible systematic temperature errors of 1.5 K. This is particularly important for the "scalar" rotational terms of the type $2(0, 0A_1)$, which correspond to a second-order Herman–Wallis correction. The $0(0, 0A_1)$ terms are influenced primarily through the partition sum. "Tensorial" terms of the type $1(1, 0F_1)$, $2(2, 0E)$, or $2(2, 0F_2)$ are less sensitive to temperature since they depend on rotation–vibration interactions independent of rotational populations or on relative populations within a given J manifold where the splittings are very small compared to kT.

The updated parameter input files for the STDS package (*24*) are available from the web site http://www.u-bourgogne.fr/LPUB/methane/metspec.htm or from the authors (J.P.C.). New calculated line parameters will be submitted to the HITRAN and GEISA databases (*25, 26*).

6. CONCLUSION

The intensities of the pentad band systems of $^{12}CH_4$ and $^{13}CH_4$ have been reanalyzed in the framework of the tensorial effective Hamiltonian approach using better data. The consistency of all available data was carefully checked to assess reliable estimates of accuracy and absolute precision of the calculated line parameters. The theoretical model for pentad transition moments did not reveal any significant divergence up to $J = 20$ for which measurements were available. After two decades of effort, there will be a calculated database that will be complete for all the bands in the 3–5 μm region arising from

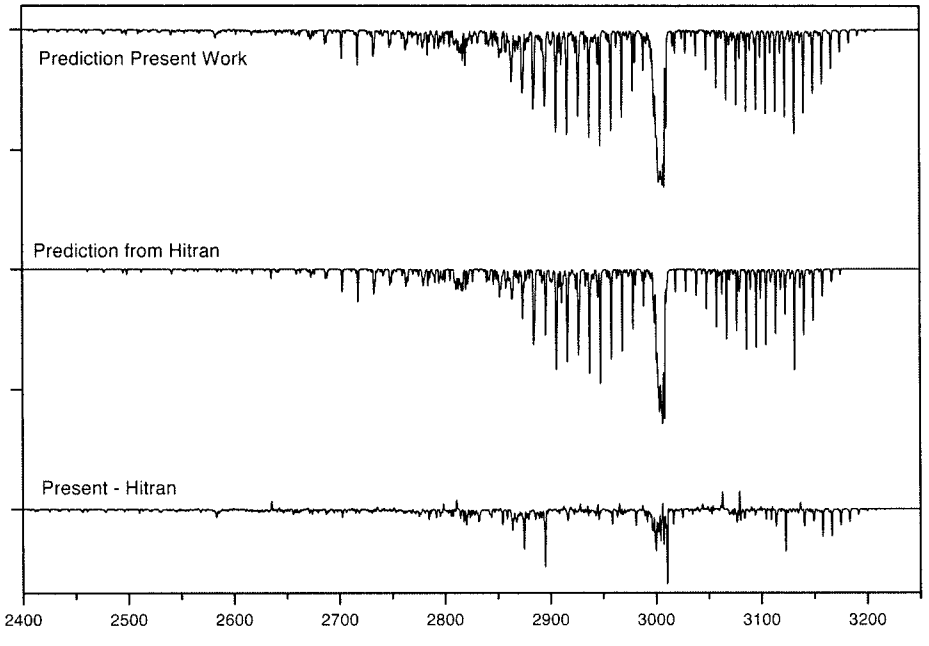

FIG. 5. Low-resolution comparison present/HITRAN $^{13}CH_4$.

the ground states of the three main isotopes up to $J = 25$ for $^{12}CH_4$ and $J = 20$ for $^{13}CH_4$ and $^{12}CH_3D$, these J limits representing reasonable extrapolations of the range of the data fitted. Figure 5 illustrates the corrections of the $^{13}CH_4$ line parameters in the HITRAN or GEISA databases. The reader is referred to Ref. (*14*) for details on the $^{12}CH_3D$ isotope.

The strongest lines of the ν_3 fundamental band of $^{12}CH_4$, which are the most important for terrestrial remote sensing, are modeled and predicted to the accuracy required by the state-of-the-art technology. The new data removes intensity offsets of 11% (from +6 to −5%) for the weaker bands which were present in the intensity measurements from the 1970s. Work is in progress to study the hot bands between 3–5 μm as was done by Ouardi *et al.* (*27*) in the dyad region.

ACKNOWLEDGMENTS

Support from the Région Bourgogne for the Dijon laboratory computer equipment and from the French INSU (Programme National de Chimie Atmosphrique) are gratefully acknowledged (J.P.C.). Part of the research reported in this paper was performed at the Jet Propulsion Laboratory, California Institute of Technology, under contract with the National Aeronautics and Space Administration (L.R.B.). Part of the research was also supported by the NASA Upper Atmosphere Research Program (A.S.P.).

REFERENCES

1. D. E. Burch and D. Williams, *Appl. Opt.* **1,** 587–594 (1962).
2. S. Saki, M. Mizuno, and S. Kondo, *Spectrochim. Acta, Part A* **32,** 403–413 (1976).
3. S. Gherissi, L. Henry, M. Lote, and A. Valentin, *J. Mol. Spectrosc.* **86,** 344–356 (1981).
4. M. Dang-Nhu, A. S. Pine, and A. G. Robiette, *J. Mol. Spectrosc.* **77,** 57–68 (1979).
5. G. Pierre, J. P. Champion, G. Guelachvili, E. Pascaud, and G. Poussigue, *J. Mol. Spectrosc.* **102,** 344–360 (1983).
6. G. Guelachvili, *Nouv. Rev. Opt. Appl.* **3,** 317–336 (1972).
7. L. S. Rothman, *Appl. Opt.* **20,** 791–796 (1981).
8. R. A. Toth, L. R. Brown, R. H. Hunt, and L. S. Rothmann, *Appl. Opt.* **20,** 932–935 (1981).
9. J. C. Hilico, J. P. Champion, S. Toumi, V. G. Tyuterev, and S. A. Tashkun, *J. Mol. Spectrosc.* **168,** 455–476 (1994).
10. A. S. Pine, *J. Opt. Soc. Am.* **66,** 97–108 (1976).
11. A. S. Pine, *J. Chem. Phys.* **97,** 773–785 (1992).
12. A. S. Pine, *J. Quant. Spectrosc. Radiat. Transfer* **57,** 157–176 (1997).
13. J. M. Jouvard, B. Lavorel, J. P. Champion, and L. R. Brown, *J. Mol. Spectrosc.* **150,** 201–217 (1991).
14. A. Nikitin, J. P. Champion, V. G. Tyuterev, L. R. Brown, G. Mellau, and M. Lock, *J. Mol. Struct.* **00,** 000–000 (1999).
15. J. P. Champion, M. Loete, and G. Pierre, *in* "Spectroscopy of the Earth's Atmosphere and Interstellar Medium" (K. N. Rao and A. Weber, Eds.), pp. 339–422, Academic Press, Columbus, 1992.
16. J. P. Champion, *Can. J. Phys.* **55,** 1802–1828 (1977).
17. M. Loete, *Can. J. Phys.* **61,** 1242–1259 (1983).
18. M. Loete, *Can. J. Phys.* **66,** 17–25 (1987).
19. V. I. Perevalov, O. M. Lyulin, V. G. Tyuterev, and M. Loete, *J. Mol. Spectrosc.* **149,** 15–33 (1991).
20. L. R. Brown, J. S. Margolis, R. H. Norton, and B. D. Stedry, *Appl. Spectrosc.* **37,** 287–292 (1983).
21. D. J. E. Knight, G. J. Edwards, P. P. Pearce, and N. R. Cross, *IEEE Trans. Instrum. Meas.* **29,** 257–264 (1980).
22. C. R. Pollock, F. R. Petersen, D. A. Jennings, J. S. Wells, and A. G. Maki, *J. Mol. Spectrosc.* **99,** 357–368 (1983).
23. K. Kim, *J. Quant. Spectrosc. Radiat. Transfer* **37,** 107–110 (1987).
24. C. Wenger and J. P. Champion, *J. Quant. Spectrosc. Radiat. Transfer* **59,** 471–480 (1998).
25. L. S. Rothman, C. P. Rinsland, A. Goldman, S. T. Massie, D. P. Edwards, J. M. Flaud, A. Perin, C. Camy-Perret, V. Dana, J. Y. Mandin, J. Schroeder, A. McCann, R. R. Gamache, R. B. Wattson, K. Yoshino, K. V. Chance, K. W. Jucks, R. H. Tipping, L. R. Brown, V. Nemtchinov, and P. Vanarasi, *J. Quant. Spectrosc. Radiat. Transfer* **60,** 665–710 (1998).
26. N. Jacquinet-Husson, E. Ari, J. Ballard, A. Barbe, L. R. Brown, B. Bonnet, C. Camy-Peyret, J. P. Champion, A. Chdin, A. Chursin, C. Clerbaux, G. Duxbury, J. M. Flaud, N. Fourri, A. Fayt, G. Graner, R. Gamache, A. Goldman, V. Golovko, G. Guelachvili, J. M. Hartmann, J. C. Hilico, G. Lefvre, O. V. Naumenko, V. Nemtchinov, D. A. Newnham, A. Nikitin, J. Orphal, A. Perrin, D. C. Reuter, L. Rosenmann, L. S. Rothman, N. A. Scott, J. Selby, L. N. Sinitsa, J. M. Sirota, A. M. Smith, K. M. Smith, V. G. Tyuterev, R. H. Tipping, S. Urban, P. Vanarasi, and M. Weber, *J. Quant. Spectrosc. Radiat. Transfer* **62,** 205–254 (1999).
27. O. Ouardi, J. C. Hilico, M. Lote, and L. R. Brown, *J. Mol. Spectrosc.* **180,** 311–322 (1996).